

PAPER • OPEN ACCESS

## A 3D discrete-element model for simulating liquid feeding during dendritic solidification of steel

To cite this article: Yi Feng *et al* 2019 *IOP Conf. Ser.: Mater. Sci. Eng.* **529** 012031

View the [article online](#) for updates and enhancements.

# A 3D discrete-element model for simulating liquid feeding during dendritic solidification of steel

Yi Feng<sup>1</sup>, Miha Založnik<sup>2</sup>, Brian Thomas<sup>3</sup>, André Phillion<sup>1</sup>

<sup>1</sup>Department of Materials Science and Engineering, McMaster University, Hamilton, Canada

<sup>2</sup>Université de Lorraine, CNRS, IJL, F-54000 Nancy, France

<sup>3</sup>Department of Mechanical Engineering, Colorado School of Mines, Golden, USA

E-mail: [andre.phillion@mcmaster.ca](mailto:andre.phillion@mcmaster.ca)

**Abstract.** A 3D meso-scale discrete-element model has been developed to simulate fluid flow during dendritic solidification of steel. The model domain is a representative volume element consisting of a set of equiaxed dendritic grain envelopes along with extra-dendritic liquid channels, where the final grain shape is given by a Voronoi tessellation. Solidification of each grain is simulated via a volume average approach. The output of the solidification simulation at a given solid fraction is used as the input mesh for the fluid flow simulation. A single domain Darcy-Brinkman model is used to calculate the pressure field within the liquid channels, with Poiseuille flow assumed to occur in the extra-dendritic region, and Darcy flow assumed to occur within the dendrite envelope. Mass conservation over each element is then used to derive a flow equation that is solved via the finite element method. The results of this new model are first compared with a previously-developed granular model [1] where fluid flow only occurs between the grains, and then compared with different forms of the Carman-Kozeny equation. It is shown that the intra-dendritic liquid fluid flow plays a major role in the semi-solid pressure field, and thus needs to be included when investigating hot tearing susceptibility in engineering alloys undergoing dendritic solidification.

## 1. Introduction

Crack formation during solidification is a serious problem in many casting processes including the continuous casting of steel slabs. During the casting process, the volume change of the solidifying metal due to the liquid to solid phase transformation as well as deformation of the semisolid mush needs to be compensated by the convection of liquid metal through the dendritic network [2]. The friction on the liquid when going through the dendritic channels leads to a pressure drop that can form a hot tear if the loss of pressure is too great [2, 3]. Transverse surface cracks observed in the cast slab section may start with the occurrence of hot tears near the meniscus [4], which are often found along the boundaries of "blown grains" [5]. After they initiate near the meniscus region in the mold, these cracks grow lower in the caster when the temperature drops into the lower-temperature ductility trough at  $\sim 700\text{--}900^\circ\text{C}$ , especially on the inner radius during unbending, where strain is large. Hot tearing is an important initial step in the formation of these detrimental cracks, which deserves more study.

Whether the microstructure is dendritic, globular, or cellular, understanding fluid flow within liquid channels of a semisolid is critical for predicting hot tearing formation. During steel solidification, the microstructure evolves from equiaxed cellular to columnar cellular to columnar



dendritic during the initial solidification. Recently a set of discrete-element or granular models of fluid flow [1, 6, 7] were proposed to investigate flow localization at the grain boundaries as part of multi-physics models of hot tearing. These models assumed that the microstructure consisted of equiaxed-globular grains, considered only fluid flow between the grains, and modeled the fluid as Poiseuille flow. For the dendritic structure found in steel, fluid flow occurs both in the extra-dendritic region between grains as well as intra-dendritic zone. The friction encountered when fluid flow occurs through dendrites may accelerate hot tear formation.

In this present work, a 3D discrete-element model is presented to simulate fluid flow within the equiaxed dendritic structure of steel. The severe temperature gradient near the meniscus, and the transformation from equiaxed grains at the surface to columnar grains are neglected. The steel selected for analysis is an alloy steel having an equivalent carbon content of 0.07 wt.%. This is a low carbon alloy that solidifies between 1532-1503 °C. The concept of equivalent carbon simplifies the solidification simulation from a five element problem to a binary one, reducing significantly computational cost. First, the methodology for creating semi-solid equiaxed-dendritic grains is reviewed along with the corresponding solidification model. Second, the new dendritic liquid feeding model is described. Third, the pressure contours and velocity within the liquid channel predicted by the new dendritic fluid flow model are compared with the previous model for equiaxed-globular grains. Finally, the results are discussed in the context of hot tearing.

## 2. Meso-Scale Solidification Model for Dendritic Alloys

As a first step in modeling the initial solidification of steel, a meso-scale model domain of 1000 grains was chosen, shown in Fig. 1(a). The empty space within the domain represents the liquid outside the envelope. To create this geometry, a Voronoi tessellation is applied to approximate the final grain morphology based on randomly-placed seeds acting as nuclei for equiaxed-dendritic grains. Each grain, Fig. 1(b), is made up of polyhedral structures, Fig. 1(c), that are further divided into tetrahedral elements.

Given that the microstructure of steels is dendritic, the evolution in solid fraction in the interior of the envelope within each tetrahedral element is predicted using a volume average approach [8]. The main idea of this approach is that each semisolid grain contains not two phases (solid and liquid) but instead three phases, delta-ferrite  $g_\delta$ , intra-dendritic liquid  $g_l^{id}$ , and extra-dendritic liquid  $g_l^{ed}$ . The sum of the volume fraction of each phase is equal to unity,  $g_\delta + g_l^{id} + g_l^{ed} = 1$ . As proposed by Rappaz and Thevoz [9] the dendrite envelope represents the region enclosed by linking the dendrite tips, and thus the intra-dendritic liquid consists of all the liquid between the dendrite arms. The volume fraction of the dendrite envelope is the sum of the solid and the intra-dendritic liquid phases,  $g_g = g_\delta + g_l^{id}$ . Temperature within each grain is assumed to be uniform and the evolution of each phase is predicted by solving explicitly the master equations given in Ref. [8]. Note that solidification within each tetrahedral element is simulated independently, and solute exchange between the neighbouring elements is neglected. All of the tetrahedral elements are then combined to create the semisolid geometry shown in Fig. 1(a) which will be used for the fluid flow calculation.

## 3. Meso-scale Fluid Flow Model for Dendritic Alloys

Fluid flow within a semisolid occurs between all the grains that have not yet coalesced. In the case of equiaxed-dendritic structures, flow occurs both in the extra-dendritic and intra-dendritic regions as can be seen in Fig. 1(d). This fluid velocity through this composite can be described by the average form of the Navier-Stokes momentum equation over a small control volume  $V$  that is large enough to smooth the morphological complexities but small enough to capture the global transport properties. Detailed derivations of the master equation and information regarding the averaging concepts can be found in Ref. [10].

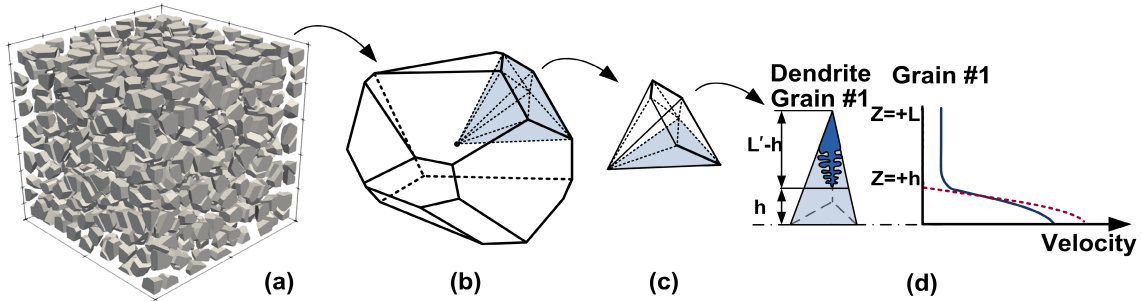


**Figure 1.** (a) Meso-scale simulation domain with 1000 grains; (b) Single Voronoi grain; (c) Polyhedral structure; (d) Tetrahedral element with dendrite, and the corresponding fluid velocity profile (blue line). In (d), the fluid velocity profile from the prior equiaxed-globular case (red line) is also shown for comparison purposes.

In the extra-dendritic region, fluid flow is similar to the case of equiaxed-globular gains, however, the no-slip boundary condition at the dendrite envelope interface (when  $z=+h$  in Fig. 1(d)) is no longer valid. Assuming quasi-steady-state, the flow is described as Poisuille flow,

$$-\nabla p + \mu_l \frac{d^2 \vec{v}^{ed}}{dz^2} = 0, \text{ and } -g'_l \nabla p + \mu_l \frac{d^2 \vec{v}^{id}}{dz^2} - \frac{\mu_l g'_l}{K(g'_l)} \vec{v}^{id} = 0, \quad (1)$$

where  $\mu_l$  represents the dynamic viscosity,  $\vec{v}^{ed}$  is the fluid velocity in the extra-dendritic region,  $p$  is the pressure.  $g'_l$  represents the local volume fraction of liquid,  $\vec{v}^{id}$  is the fluid velocity vector within the dendrite envelope and  $K(g'_l)$  represents the individual hydrodynamic permeability as a function of liquid fraction. The Carman-Kozeny equation [11] is used to determine the permeability within each tetrahedral element. Assuming that  $\frac{\partial}{\partial z} \vec{v}|_{z=0} = 0$  and  $\vec{v}$  is finite when  $z \rightarrow \infty$ , Eq. 1 can be solved analytically,

$$\vec{v}^{ed} = \left( \frac{z^2}{2\mu_l} + C_1 \right) \nabla p, \text{ and } \vec{v}^{id} = \left( C_2 e^{\frac{z}{\delta}} - C_3 \right) \nabla p. \quad (2)$$

In Eq. 2,  $C_1$  and  $C_2$  represent two unknown constants,  $C_3 = \frac{g'_l \delta^2}{\mu_l}$  and  $\delta = \sqrt{\frac{K(g'_l)}{g'_l}}$ . The unknown constants can be further solved with additional constraints. Since all of the fields are continuous within the whole domain, the velocity and the viscous stress at the interface between the intra-and extra-dendritic regions must be continuous. Then,

$$C_1 = -\frac{\delta h}{\mu_l} - \frac{g'_l \delta^2}{\mu_l} - \frac{h^2}{2\mu_l}, \text{ and } C_2 = \frac{-\frac{\delta h}{\mu_l}}{e^{-\frac{h}{\delta}}}. \quad (3)$$

By integrating the above equations over two facing tetrahedral elements, with symmetry plane shown by the dotted line in Fig. 1(d), one then obtains the flux; then using the divergence theorem and the Green's theorem, the equation for dendritic flow can be obtained:

$$\left[ \left( \frac{h^3}{3\mu_l} + 2C_1 h \right) S_1 + 2 \left( C_2 \delta e^{-\frac{h}{\delta}} + C_3 h - C_2 \delta e^{-\frac{L'}{\delta}} - C_3 L' \right) S_2 \right] \nabla^2 p = 0, \quad (4)$$

where  $S_1$  and  $S_2$  are dendrite envelope area and solid/liquid interface area based on the equivalent solid radius, respectively, and  $L'$  is the total length of grain.

A schematic of the resulting fluid flow in one dendrite is given in Fig. 1(d) (blue line). For comparison purposes, the flow prediction from the equiaxed-globular case is also given (red line). In this second curve, flow only occurs in the intergranular region, and thus for a given fluid flux the maximum velocity must be greater in order to displace an equivalent amount of fluid in a given time. For the entire domain, the fluid flow mesh consists of triangular prismatic elements representing the liquid phase of each tetrahedral element with connectivity provided by the solidification model. The finite element solution of Eq. 4 is achieved following the procedure outlined Ref. [1].

#### 4. Results and Discussion

Below, a set of simulations are presented to compare the influence of microstructure on the fluid flow within the dendritic and globular structures at different solid fractions where the extra-dendritic liquid channel widths for the dendritic structure are approaching zero due to the high cooling rate of  $50\text{ }^{\circ}\text{C}\cdot\text{s}^{-1}$ , and secondary armspacing is selected to be  $33\text{ }\mu\text{m}$ . The domain was  $5\text{ mm}\times 5\text{ mm}\times 5\text{ mm}$  consisting of 1000 grains, and  $\mu_l = 7.0 \times 10^{-3}\text{ Pa}\cdot\text{s}$ . For the bulk permeability assessment, an isothermal flow simulation is conducted using the following boundary conditions: a constant pressure on the top surface,  $p_t = 0\text{ Pa}$ , a constant non-zero flux on the bottom surface,  $q_b = 50\text{ }\mu\text{m}\cdot\text{s}^{-1}$  and closed lateral surfaces,  $q_s = 0\text{ }\mu\text{m}\cdot\text{s}^{-1}$ .

##### 4.1. Fluid Flow

Pressure contours within the liquid channels obtained from the two models are shown in Fig. 2. For better visibility, the grains are shaded with the same colour of the pressure in the liquid channel. First, it can be seen that a lower pressure is obtained at a further distance away from the top of the domain. Second, a higher pressure drop was found in the dendritic microstructure as compared with the globular structure. This is because the increased fluid friction in the dendritic network will require a larger pressure drop to achieve the same fluid flow. Although not shown, the localization of the liquid feeding along several preferential channels can be observed in the velocity contours. Since the permeability of the dendritic structure is lower than that of globular structure at the same solid fraction, the maximum velocity within the liquid channels is also lower, being  $162\text{ }\mu\text{m}\cdot\text{s}^{-1}$ , in the dendritic structure as compared to  $5949\text{ }\mu\text{m}\cdot\text{s}^{-1}$  in the globular structure.

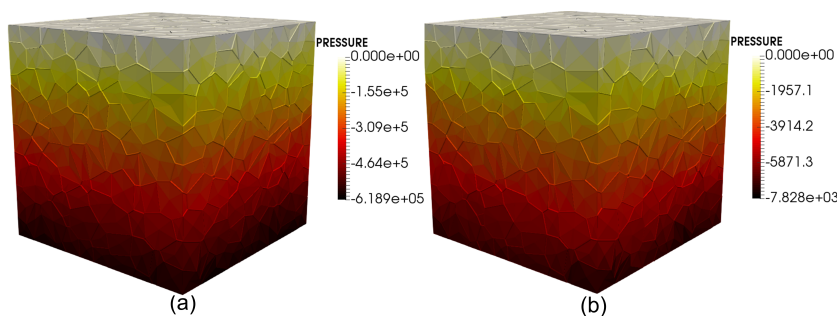


**Figure 2.** Pressure distribution at a solid fraction of 0.95: (a) dendritic and (b) globular.

##### 4.2. Hot Tearing Sensitivity Coefficient

It is well known that pressure gradient within a semisolid domain is a contributing factor to hot tearing sensitivity [1]. The pressure gradient itself can be utilized as a sensitivity coefficient.

Fig. 3(a) compares the hot tearing sensitivity coefficients for both the dendritic and globular structures. As can be seen, the values are rather low at low solid fraction due to the adequate liquid feeding; hot tearing is unlikely to occur. At high solid fraction, there is an increase in the sensitivity coefficient however the sharp rise occurs both earlier in the dendritic structure and to a much greater extent as compared to the globular structure. Thus, the model shows

that hot tearing is more prevalent in dendritic structures because the increased difficulty in fluid flow increases the pressure drop within the semisolid and increases hot tearing susceptibility at a given solid fraction.

#### 4.3. Model Verification

Finally, the dendritic fluid flow model can be verified by comparing its predictions of permeability against the analytical Carman-Kozeny equation. For this comparison, a brief review of the Carman-Kozeny equation is useful. The local permeability shown in Eq. 1 can be calculated from the local fraction liquid and the solid/liquid interfacial area concentration  $S_v$ ,

$$K = \frac{(g'_l)^3}{5S_v^2}. \quad (5)$$

$S_v$  is influenced by grain growth, impingement and coarsening processes [12], and can be approximated in one of two ways, by assuming a one-dimensional platelike geometry of the secondary dendrite arm [13], or through an empirical link with solid fraction [12]). These are shown below, where  $\lambda_2$  is the cooling-rate dependent [14] SDAS, and  $c$ ,  $p$  and  $q$  are constants [12, 15],

$$S_v = \frac{2}{\lambda_2}, \quad (6)$$

$$S_v = cg_s^p(1 - g_s)^q. \quad (7)$$

For the verification, simulations at different solid fraction were performed using the same conditions.  $K$  is then calculated as,

$$K = \mu_l \frac{q_b}{\left(\frac{p_t - p_b}{L}\right)}, \quad (8)$$

where  $L$  is the distance between the two surfaces, and  $p_b$  is the bottom surface pressure.

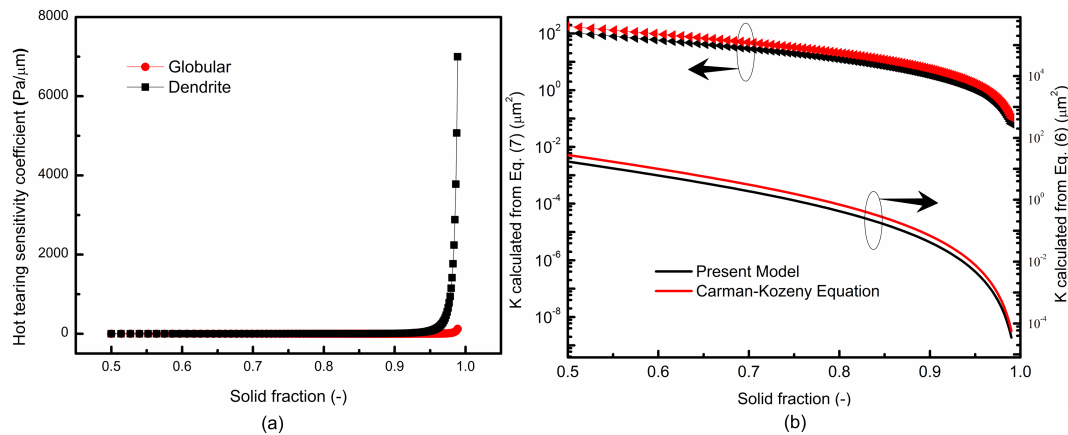


**Figure 3.** (a) Variation in hot tearing sensitivity coefficient with solid fraction in both dendritic and globular structure. (b) Permeability comparisons for the two  $S_v$  terms.

Fig. 3(b) shows the evolution in bulk permeability predicted by the model and Carman-Kozeny equation for both  $S_v$  equations, a good match has been achieved. All the curves display similar trends where the permeability decreases with increasing solid fraction, and the gap between any two curves narrows near the end of solidification as the liquid fraction within the dendrite envelope  $\rightarrow 0$  and thus the remaining liquid must flow around the grains. Further,

a higher value in permeability is always predicted by Carman-Kozeny, irrespective of  $S_v$ . This might be due to the assumption that the fluid flow direction is always parallel to the bottom surface of tetrahedral element, resulting in lower permeability due to the increased friction forces. The different  $S_v$  equations also predict significantly different values of permeability, with the method based on SDAS being nearly three orders of magnitude smaller at the end of solidification.

## 5. Conclusions

Preliminary work to model grain structure effects related to hot tearing during steel solidification was carried out, where the fluid flow behaviour within semisolid steel having a composition of 0.07 wt.%C with dendritic microstructure has been predicted at the meso-scale. First, the semisolid microstructure in an ensemble of grains was created using a volume average approach to model solidification of individual grain. Each grain consists of three phases, delta-ferrite, intra-dendritic liquid, and extra-dendritic liquid in order to simulate the dendritic structure. Second, at a prescribed solid fraction, the Darcy-Brinkman form of the Navier-Stokes equation was used to predict fluid flow between and through the grains. The extra-dendritic position was treated as a pure liquid zone, while the region within the dendrite envelope was treated as a porous medium. The results of the new dendritic fluid flow model have been compared to a previous model consisting of globular microstructure [1], as well as the well-known Carman-Kozeny equation. It is shown that, for a given solid fraction, dendritic microstructure undergoes a higher pressure drop than globular microstructure. This difference is due to the fluid friction occurring within the dendrite envelope; this friction is not present in globular microstructure. The Carman-Kozeny also over-estimates the permeability for the same reasons. A hot tearing sensitivity coefficient was developed, demonstrating that the increased hot tearing susceptibility in dendritic structures is a result of an increase in the difficulty for fluid flow to occur.

Future work would focus on the application of present model to the meniscus of casting steel by simulating the fluid flow behavior within a domain containing a few grains, and predict the initiation of hot tearing by imposing the strain on the domain.

## Acknowledgements

The authors wish to thank the Natural Sciences and Engineering Research Council of Canada (NSERC) and the McMaster Steel Research Centre for financial support.

## References

- [1] Sistaninia M, Phillion A, Drezet J M and Rappaz M 2012 *Acta Materialia* **60** 3902–3911
- [2] Rappaz M, Drezet J M and Gremaud M 1999 *Metallurgical and materials transactions A* **30** 449–455
- [3] Flemings M C 2006 *Materials Science and Technology*
- [4] Mišičko R, Fujda M, Fedáková S, Fedáková D and Szekeres S 2012 Further study of the "blown grains" condition
- [5] Szekeres E 2002 A review of strand casting factors affecting transverse cracking *Proceedings of 6th International Conference on Clean Steel* pp 324–338
- [6] Vernede S, Jarry P and Rappaz M 2006 *Acta Materialia* **54** 4023–4034
- [7] Rajani H Z and Phillion A 2018 *Materials & Design* **144** 45–54
- [8] Tourret D and Gandin C A 2009 *Acta Materialia* **57** 2066–2079
- [9] Rappaz M and Thevoz P 1987 *Acta Metallurgica* **35** 1487–1497
- [10] Le Bars M and Worster M G 2006 *Journal of Fluid Mechanics* **550** 149–173
- [11] Bear J 2013 *Dynamics of fluids in porous media* (Courier Corporation)
- [12] Neumann-Heyme H, Eckert K and Beckermann C 2017 *Acta Materialia* **140** 87–96
- [13] Wang C, Ahuja S, Beckermann C and De Groh H 1995 *Metallurgical and Materials Transactions B* **26** 111–119
- [14] El-Bealy M and Thomas B G 1996 *Metallurgical and materials transactions B* **27** 689–693
- [15] Domitner J, Kharicha A, Wu M and Ludwig A 2013 *Metallurgical and Materials Transactions A* **44** 607–616